Article

Flexible Micro-Structured Capacitive Pressure Sensors by Laser Engraving and Graphitization from Natural Wood

Chenkai Qu , Meilan Lu , Ziyan Zhang , Shangbi Chen , Dewen Liu , Dawei Zhang , Jing Wang , Bin Sheng *

Posted Date: 18 May 2023

doi: 10.20944/preprints202305.1313.v1

Keywords: laser induced graphene; flexible pressure sensor; micro-structures; capacitance sensors; laser engraving

Article

Flexible Micro-Structured Capacitive Pressure Sensors by Laser Engraving and Graphitization from Natural Wood

Chenkai Qu [1,2], Meilan Lu [1,2], Ziyan Zhang [1,2], Shangbi Chen [3], Dewen Liu [3], Dawei Zhang [1,2], Jing Wang [4] and Bin Sheng 1,2, *

[1] School of Optical Electrical and Computer Engineering, University of Shanghai for Science and Technology, Shanghai 200093, China; 1935031916@st.usst.edu.cn (C.Q.); 1935030804@st.usst.edu.cn (M.L.); 1935030808@st.usst.edu.cn (Z.Z.); dwzhang@usst.edu.cn (D.Z.)

[2] Shanghai Key Laboratory of Modern Optical Systems, Engineering Research Center of Optical Instruments and Systems, Shanghai 200093, China

[3] Shanghai Aerospace Control Technology Institute, Shanghai 201109, China; chensb@mail.ustc.edu.cn(S.C.); dewerl@126.com (D.L.)

[4] Department of Ultrasound Medicine, The First Affiliated Hospital, Zhejiang University School of Medicine, Hangzhou, China; yanshu006@zju.edu.cn (J.W.)

* Correspondence: bsheng@usst.edu.cn

Abstract: In recent years, laser engraving has received widespread attention as a convenient, efficient, and programmable method, which has enabled the obtaining of high-quality porous graphene from various precursors. Laser engraving is often used to fabricate the dielectric layer with micro-structure for capacitive pressure sensors, however, the usual choice of electrodes remains poorly flexible metal electrodes, which greatly limits the overall flexibility of the sensors. In this work, we propose a flexible capacitive pressure sensor made entirely of thermoplastic polyurethane (TPU) and laser-induced graphene (LIG) derived from wood. The capacitive pressure sensor consisted of a flexible LIG/TPU electrode (LTE), a LIG/TPU electrode with micro hole array, and dielectric layer of TPU with micro-cone array molded from laser-engraved hole array on wood, which provided high sensitivity (0.11 kPa^{-1}), ultra-wide pressure detection range (100Pa to 1.4MPa), fast response (~300 ms) and good stability (>4000 cycles, at 0-35 kPa). We believe that our research makes a significant contribution to the literature because the easily available materials derived from wood and overall consistent flexibility meet the requirements of flexible electronic devices.

Keywords: laser induced graphene; flexible pressure sensor; micro-structures; capacitance sensors; laser engraving

1. Introduction

Flexible pressure sensors that are increasingly paid more attention because of flexibility, lightweight and stretching is crucial to a wide range of applications in surgical operation [1-4], moisture detection [5-10], human motion [11-14], and wearable devices [15-17], etc. According to various working mechanisms, flexible pressure sensors can be divided to resistivity [10, 18-19], capacitance [20-22], triboelectricity [23], and piezoelectricity [24,25]. Among them, capacitive flexible sensors have been studied extensively by researchers because of their simple structure, easy assembly and wide range of application [20-22, 26]. A large number of micro-structures comprising of micro-pyramids, micro-domes, semi-cylinders, porous structure, etc. are applied for improving sensitivity of capacitive pressure sensors [20,22,26-32]. Since most microstructures are manufactured using processes such as photolithography, PVC, etc., their processes are complicated, expensive and time-consuming [28,30]. As an emerging method, laser engraving has received a lot of attention to fabricate micro-structure because of its higher accuracy, simpler process and more convenience than traditional methods [27,33].

 doi:10.20944/preprints202305.1313.v1

In addition to processing methods as fabricating microstructure, laser engraving is also capable to fabricate Laser-Induced Graphene (LIG) on diverse precursors ranging from polymers or renewable precursors like cloth, paper, and woods, etc. [18,34-39] LIG, as an excellent porous 3D graphene-based nanomaterial, is obtained easily from materials such as polyimide (PI), polydimethylsiloxane (PDMS), or polyurethane for strain, temperature, and humidity detection [36,40-44]. LIG transferring with elastic materials has also been shown high performance in supercapacitors, physical/chemical sensors, etc. [42,45-48] However, for most of the LIG layers that are peeled by elastic materials, the process often requires assembly with extra electrodes to become a complete capacitive sensor, but the curing of the adhesive often affect the use of sensors when the flexible sensor is squeezed and stretched by external forces. It causes that the adhesive between the electrodes and metal materials of electrodes, such as copper, silver et. al., become a major limitation that influences the flexibility and durability of the capacitive sensor [21]. It seems possible to employ dependable, flexible adhesives. Moreover, the simultaneous molding of the electrode and the dielectric layer appears to be a simpler and more efficient method. It is easy to think of LIG as a conductive substance that can be applied, so it is likely that the resistance of the LIG is small enough to be used as an electrode.

In this work, we have successfully realized the integration of LIG electrode and LIG electrode with laser-engraved microstructure by secondary laser engraving on wood and peeling it off by thermoplastic polyurethane(TPU). We demonstrated that minimizing the ablative effect can improve the amount of LIG generated by pretreating the wood with flame retardant treatment in order to make the resistance of LIG generated by laser scribe modest enough. Using laser engraving, we also produced micro-cone structure on a LIG electrode rapidly and simply, which significantly increases the sensor's sensitivity. The capacitive pressure sensor consisted of a flexible LIG/TPU electrode (LTE), a LIG/TPU electrode with micro hole array, and dielectric layer of TPU with micro-cone array molded from laser-engraved hole array on wood, which provided high sensitivity (0.11 kPa^{-1}), ultra-wide pressure detection range (100Pa to 1.4MPa), fast response (~300 ms) and good stability (>4000 cycles, at 0-35 kPa). This method solves the flexibility problem caused by the adhesive and the electrode, and it is more economical, durable and less time-consuming and less adhensive for application.

2. Methods and Materials

2.1. Fabrication of the LTE and Micro-Cone Array Pressure Sensor

The main fabrication procedure of the LTE and micro-cone array Pressure Sensor(LMPS) is illustrated in Figure 1a. First, the planks (100% pine, ~1cm of thickness) is covered by XF-630 flame retardant of nitrogen and phosphorus (Shanghai, China) for five minutes to ensure shallow penetration depth of flame retardant and dries using a hot air blower. After drying, LTE, a LIG/TPU electrode with micro hole array, and dielectric layer of TPU with micro-cone array are both fabricated by a semiconductor laser (450nm wavelength, from DAJA, Dongguan, China). The LTE was obtained by irradiating the laser on the planks according to the set square area to form the LIG (Figure 1b), and finally coating the LIG part with the configured TPU solution (The TPU solution is prepared by mixing TPU particles with N-N dimethylformamide in the ratio of 1:3, waiting for 30 minutes to soften the TPU particles, and then stirring the solution for 30 minutes to completely mix the TPU particles with N-N dimethylformamide. The solution is placed for half an hour for the air bubbles in the solution to escape from the solution, and then it can be used as the substrate of electrode.), putting it in a vacuum drying oven for 30 minutes to make the TPU solution fully penetrate into the LIG, curing it at 80°C for 4 hours and then peeling it off. Similar to the LTE, the LIG/TPU electrode with micro hole array, and dielectric layer of TPU with micro-cone array (Figure 1c, d) is prepared by irradiating the square area with laser, then irradiating the area according to the set dot matrix, coating it with TPU solution, vacuuming it, curing it, and peeling it off as the above process.

Preprints (www.preprints.org) | NOT PEER-REVIEWED | Posted: 18 May 2023 doi:10.20944/preprints202305.1313.v1

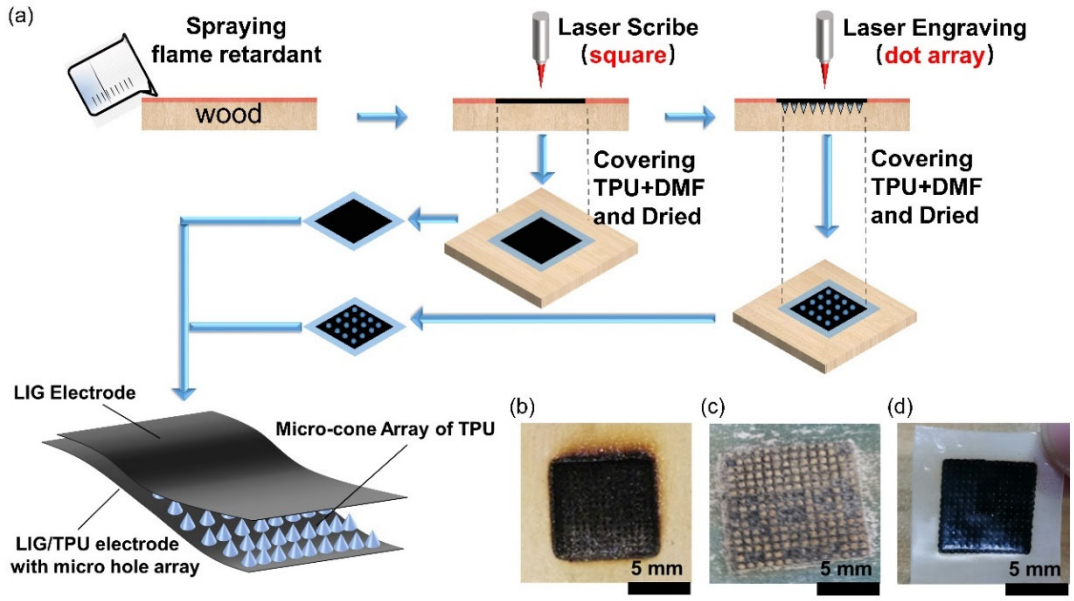

Figure 1. (a) Main fabrication procedure of pressure sensor comprising of LTE and a LIG/TPU electrode with micro hole array, and dielectric layer of TPU with micro-cone array. (b) A optical image of surface of wood after laser engraving. (c) A optical image of the LIG/TPU electrode with micro hole array, and dielectric layer of TPU with micro-cone array. (d) A optical image of the LIG/TPU electrode with micro hole array.

2.2. Performance Test of the LTE and Micro-Cone Array Pressure Sensor

The sheet resistances of the LTE were measured using a Keithley four-point probe meter (St-2253). The sheet resistance of the LTE can be obtained directly from the above machine. A high-precision single-axis electrodynamic force tester (ZQ-990B, Zhiqu Precision Instrument Co., Ltd., China) was used to compress and release the LTE and LMPS repeatedly.

The capacitance of the pressure sensor was measured at room temperature (25 °C) using a desktop digital bridge (VC4092A, Xi'an Shengli Instrument Co., Ltd., China) with a frequency of 1 kHz, a AC voltage of 3.0 V and a recording interval of 1 s. Here, the sensitivity is defined by:

$$S=(\partial(\Delta C/C0)/\partial P)$$

where C and C0 stand for the resulting capacitance and the original capacitance without the loading pressure (P).

3. Results and Discussion

3.1. Laser Operation Parameter Optimization of the LTE

Laser irradiation of natural materials such as wood and leaves can produce LIG with good performance known from previous researches [37-39], and the LIG produced by planks treated with flame retardant has significantly better resistance than that of untreated ones, as will be demonstrated later in Figure 3g. In order to know the most suitable parameters for LTE, we first conducted a comprehensive study of LTE in terms of laser power, scan speed and defocus distance. From the tests of laser power and scan speed (Figure 2a, b), we obtained a minimum sheet resistance(14.7Ω) of LIG by 48 mm s^{-1} scan speed and 50% laser power. The defocus distance based on the above data is adjusted to obtain the smallest sheet resistance LIG at ~0.5mm (Figure 2c). In order to further study the optimal sheet resistance for the parameters of scan speed, laser power and defocus distance without considering the distance from the focus, we also studied the sheet resistance for different laser powers at fixed scan speed (48mm s^{-1}) and defocus distance(~0.5mm), and it can be seen that the sheet resistance is also minimum when the parameters of the lowest sheet resistance are taken for all

Preprints (www.preprints.org) | NOT PEER-REVIEWED | Posted: 18 May 2023 doi:10.20944/preprints202305.1313.v1

three parameters (Figure 2d). The lowest sheet resistance of LIG was 14.7Ω/□. So we choose 50% laser power, 48mm s^{-1} scan speed and 0.5mm defocus distance to fabricate LTE. (The LTE and the LIG/TPU electrode with micro hole array mentioned after this paper are prepared using this parameter) In addition, as we can see from Figure 2d, the sheet resistance increases significantly after incorporating TPU. This is because TPU is an insulator, and the infiltration of TPU leads to the destruction of some of the original conductive paths of LIG, so the sheet resistance increases.

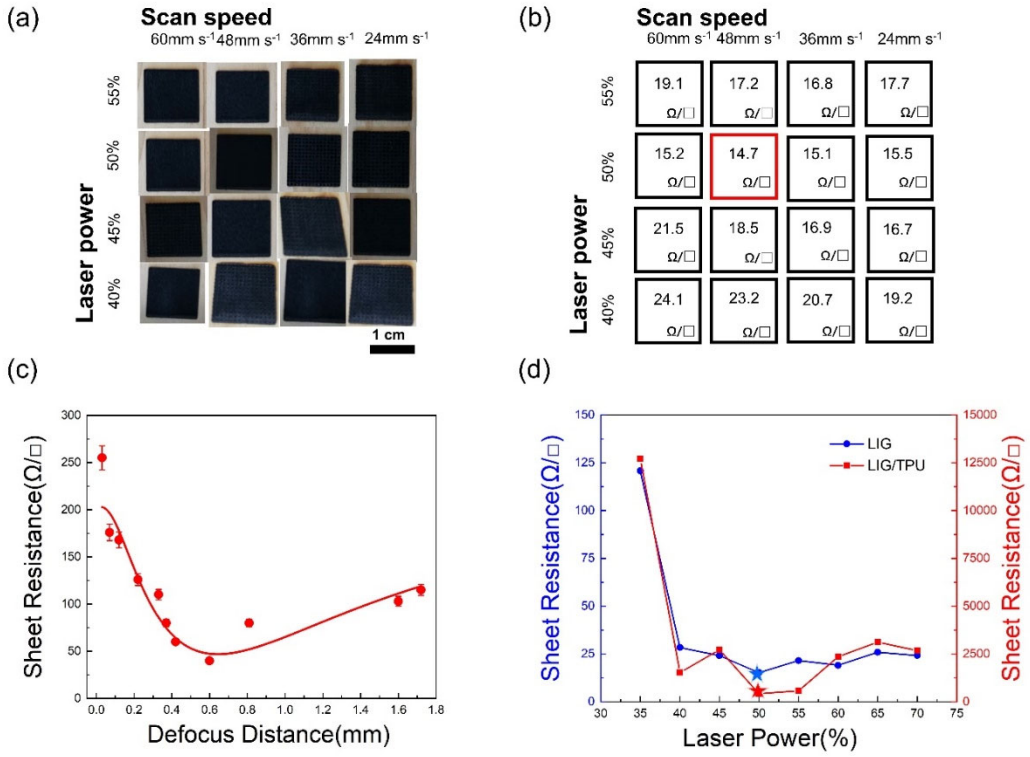

Figure 2. (a, b) LTE was engraved by different laser scan speed and power and their sheet resistance (c) The change of sheet resistance with the defocus distance in the case of 48 mm s-1 scan speed and 50% laser power (d) The sheet resistance of LIG and LIG/TPU with different laser power when scan speed 48mm s-1, defocus distance 0.5mm.

Preprints (www.preprints.org) | NOT PEER-REVIEWED | Posted: 18 May 2023 doi:10.20944/preprints202305.1313.v1

3.2. Characterization of LTE from Wood and the Effect of Flame Retardant

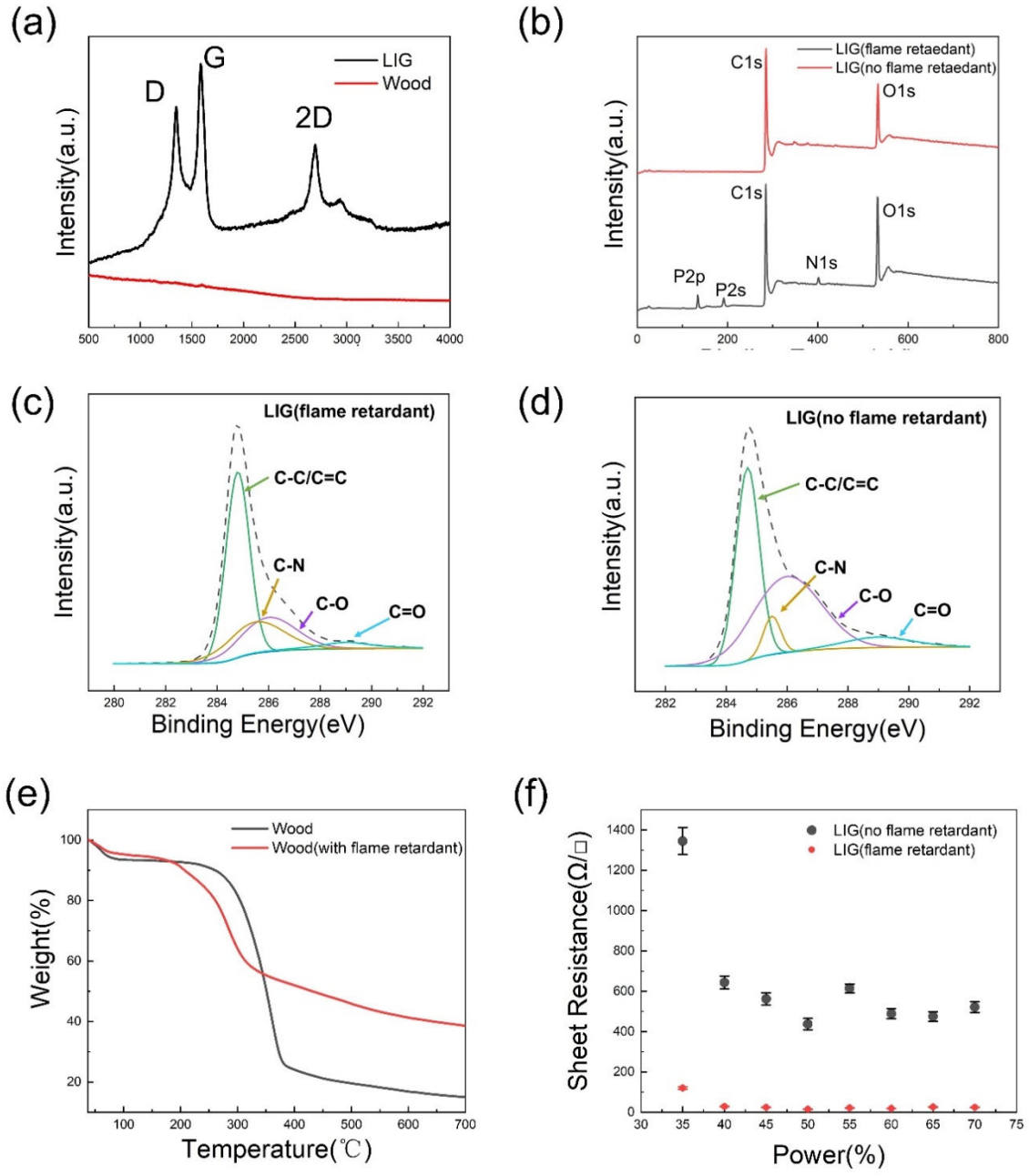

Figure 3. (a) Raman spectrums of LIG at 532nm and wood at 785nm. (b) XPS survey spectrums of the LIG (flame retardant), LIG (no flame retardant). (c, d) The detailed element information of the XPS C1s spectrums of the LIG (flame retardant), LIG (no flame retardant). (e) Thermogravimetric curves of wood and wood with flame retardant. (f) Sheet resistance of LIG between flame retardant and no flame retardant on different laser power.

To further investigate the composition of LTE and the effect of flame retardant on wood for LIG, chemical analyses of the surfaces of LTE and TPU were performed. Raman spectrums were measured with a Raman spectroscopy (WITec, Apyron) equipped with a 532 nm laser wavelength and a 785nm laser wavelength because LIG can be measured at 532nm, but wood is not measurable at 532 nm. Three distinct peaks in the Raman spectrum were visible at 1326 cm^{-1}, 1577 cm^{-1}, and 2650 cm^{-1} correspond to the D, G, and 2D bands respectively, which could show the possible graphite structure [38]. The 2D peak is not obvious, which indicates that LIG is multilayer graphene. Last but not least,

 doi:10.20944/preprints202305.1313.v1

the momentum conservation achieved by two phonons with opposite wavevectors is what causes the 2D peak at about 2700 cm^{-1} to be activated without the need for any defects. As shown in Figure 3b-e, The X-ray photoelectron spectroscopy (XPS) (Thermo Fisher Scientific K-Alpha) was performed to evaluate the detailed element information (Figure 3b). From Figure 3b, it can be seen that LIG (flame retardant) and LIG (no flame retardant) show two peaks, in which the carbon 1s peak occurred at 285 eV while the oxygen 1s peak occurred at 532 eV. For LTE mixed with flame retardant treated LIG and non-flame retardant treated LIG and TPU, the atomic ratios of carbon 1s to oxygen 1s are 1.29 and 2.08, respectively. This result indicates that the ratio of carbon atoms to oxygen atoms decreases after flame retardant treatment, which is contrary to the expected effect of flame retardant treatment. Therefore, the C1s spectrums of the two LIG samples with and without flame retardant treatment were further investigated. In addition, no nitrogen and phosphorus were detected in the LIG(no flame retardant), while the LIG(flame retardant) contained 2.55% nitrogen and 9.93% phosphorus. This is because flame retardants contain a lot of nitrogen and phosphorus elements. Figure 3c, d, exhibit that the C1s spectrums of two samples of LIG with flame retardant and without flame retardant contain 4 peaks locating at 284.7 eV (C-C/C=C), 285.5 eV (C-N), 286.0 eV (C-O), and 289.0 eV (C=O), respectively [18]. It can be clearly seen that the content of C-C/C=C bond increases from 40.9% to 51.7% by flame retardant treat-ment, while the intensities of those from oxygen-containing groups (C-O, C=O) plummet decreases from 53.0% to 27.1%, which indicates that the flame retardant treatment is effective. In addition, the content of C-N bond increases from 6.0% to 21.0%. This is mainly because the flame retardant contains N and P elements, and the content of N and P elements in the generated LIG is increased.

Thermogravimetric curves of wood and wood with flame retardant are shown in Figure 3e, indicating that the decomposition temperature of the two samples is approximate 80℃. With the heating process beyond 350℃, the wood without flame retardant displayed the faster weight loss. It indicated that ablation produces more gas, leading to a reduction in char. The remaining weight of wood with flame retardant declares that the less ablation leads to more formation of char, which is consistent to the research of flame retardant of nitrogen and phosphorus that flame retardant of nitrogen and phosphorus decomposes by heat to release nitrogen gas to isolate oxygen for flame retardant effect, and produce more char in the process [48]. The above results all prove that flame retardants are effective in avoiding ablation and are favorable for more formation of LIG to reduce the LTE's sheet resistance. (Figure 3f)

3.3. Morphology and Sensing Mechanism of the LIG/TPU Electrode with Micro Hole Array, and Dielectric Layer of TPU with Micro-Cone Array

The detailed morphology and microstructure of the LTE and micro-cone of TPU are shown in Figure 4a-d. The micro-cone of TPU is formed by secondary laser irradiation on the basis of the LTE. To facilitate the study, we set the parameters of the secondary irradiation at 50% laser power,48mm s^{-1} scan speed and 0.5mm defocus distance. We applied a scanning electron microscope to investigate the surface morphology of LTE and micro-cone of TPU. (TESCAN MIRA3). The surface of the LTE (Figure 4a) has a large amount of linear structure, which can be seen in the magnified LTE surface (Figure 4b). This is mainly due to the directional nature of the fiber structure of the wood itself and the path that the laser continuously engraves through, while the few fine hairy structures on the LTE surface may be the result of weak ablation or take down damage. Figure 4c, d shows the conical multi-level microstructure formed on the micro-cone of TPU by a single laser pulse. On the basis of the cone, there are multi-level burrlike structures at different heights, and their direction is the same as the growth direction of the wood fibers, which is caused by the ablation that occurs inside the wood without flame retardant treatment [50]. The formation of this microstructure is closely related to the laser power. The laser's power distribution is shown in Figure 4e, and it can be observed that it has a Gaussian distribution [51]. I_ω is the minimum power that the laser can transform the wood, it can be seen that the impact area is the power range greater than I_ω, and the transformation depth is proportional to the power of the laser, the higher the power the deeper the transformation depth. The laser power distribution coincides with the conical structure formed. After understanding the

Preprints (www.preprints.org) | NOT PEER-REVIEWED | Posted: 18 May 2023 doi:10.20944/preprints202305.1313.v1

principle of microstructure formation, in order to further optimize the microstructure layer, we studied the microstructure under different power based on 48mm s^{-1} scan speed, and it can be seen from Figure 4f that the height of the microstructure formed from 200μm to 1mm, we finally chose 400μm height on 55% laser power, because although the higher the height of the microstructure the higher the sensitivity of the sensor, but the higher the height of the microstructure, the lower the initial resistance of the sensor, which is not beneficial for the practical application of the sensor [32, 52].

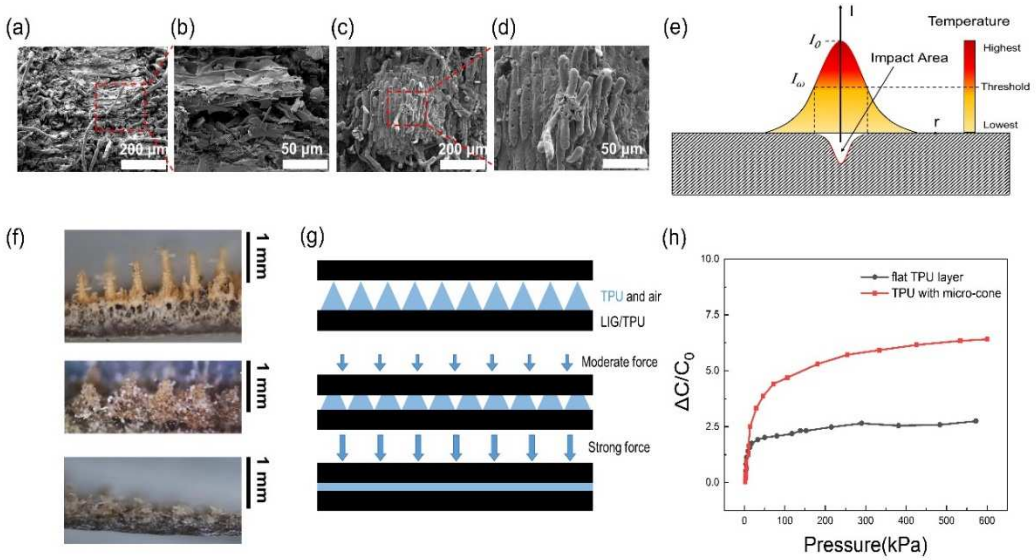

Figure 4. (a, b) SEM images of the surface of the LTE. (c, d) SEM images of the surface of micro-cone of TPU (e) A schematic of mechanism of microstructure formation by laser engraving. (f) A optical image of micro-cone fabricated by different laser powers and 48mm s-1 scan speed. (g) a schematic of the sensing mechanism for the dielectric layer with micro-cone. (h) Relative capacitance variation of TPU with micro-cone and flat TPU layer.

Figure 4g illustrates the sensing mechanism of the LMPS, which is a collection of TPU dielectric layer and LIG/TPU electrode to form a complete capacitive pressure sensor. when the electrode surface is subjected to pressure, the micro-cone will be deformed, and the distance between the electrode and the electrode will be reduced to produce the change of capacitance. The burr structure on the cone has a small effect on the sensitivity, but it increases the contact area between the LTE and the micro-cone to a certain extent, which improves the stability between the two electrodes. Due to the characteristic that the upper tip of the micro-cone is easily deformed, while the lower bottom is wide with less deformation under the same pressure, the sensitivity of the sensor is high at low pressure, when the distance between electrodes decreases and the ratio of air between electrodes decreases, the dielectric constant between electrodes increases, and the TPU ratio increases two factors which affect the capacitance increases, and the ratio of air between electrodes still decreases as the pressure keeps increasing. But the distance between the electrodes decreases becomes difficult, so the sensitivity decreases. When the pressure increases again, the air gap between the electrodes has completely disappeared, and the dielectric constant between the electrodes no longer increases, while making the distance between the electrodes more and more difficult to reduce, so the sensitivity is even lower, which is consistent with the load curve shown in Figure 5a. In order to verify the above mechanism, we prepared the same amount of TPU into a flat dielectric layer and a dielectric layer with micro-cone to measure its capacitance, and it can be seen from Figure 4h that the sensitivity is higher when the pressure is lower because the micro-cone is more likely to deform, and when the air gap between the electrodes is gradually filled, the capacitance change is exactly the same as that of the flat TPU layer.

Preprints (www.preprints.org) | NOT PEER-REVIEWED | Posted: 18 May 2023 doi:10.20944/preprints202305.1313.v1

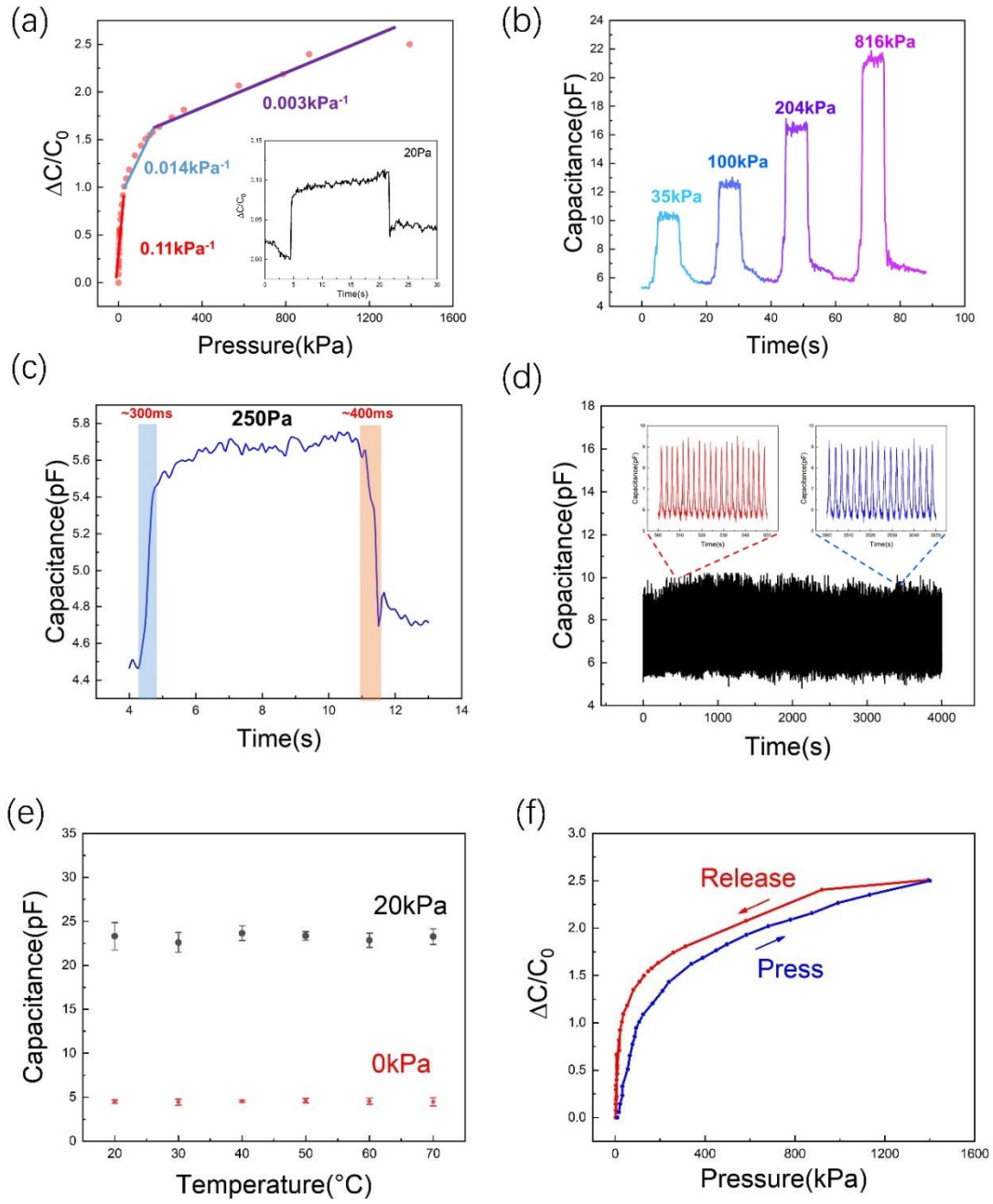

Figure 5. (a) Electrical output of the LMPS at different loadings and the minimum detection limit. (b) Recognition of different pressure variations of the proposed sensor from low pressure to high pressure. (c) The response and recovery speed of the LMPS at a loading of 250 Pa. (d) Mechanical durability of the LMPS at a loading of 35 kPa. (e)Capacitance variation of the LMPS at different temperatures under 0 kPa and 20 kPa. (f) Hysteresis response of the LMPS against pressure.

3.4. Electrical Properties of the LMPS Composed of LTE, LIG/TPU Electrode with Micro Hole Array, and Dielectric Layer of TPU with Micro-Cone Array

The LMPS consists on a LTE, a LIG/TPU electrode with micro hole array, and dielectric layer of TPU with micro-cone array. Due to the good electrical conductivity of LTE, it can be used directly as an electrode and has outstanding electrical conductivity and reliability. Under external pressure, the electrical signal of the device changes as shown in Figure 5a. The LMPS has a wide detection window of up to 1393 kPa and the minimum detection limit of ~20 Pa. The electrical response of the device (Figure 5a) can be divided into three parts with different sensitivities at different load ranges. In the

 doi:10.20944/preprints202305.1313.v1

loading range of 0.01 ~ 20 kPa, the device has a sensitivity of ~ 0.11 kPa^{-1} and the sensitivity decreases to ~ 0.014 kPa^{-1} from 20 to 155 kPa. While the loading range is 155~1393kPa, the sensitivity is ~0.003kPa^{-1}. This result shows that the LMPS has a high sensitivity at low load, which is consistent with the capacitance change caused by the deformation of the tip of the micro-cone at low load. We also tested the LMPS for rapid capacitance changes under different loading pressures, and the results showed that the LMPS can respond to the load very quickly, and the signal is stable under the load condition. (Figure 5b) The response time of compress and release of LMPS is ~300ms and ~400ms at a load of 250 Pa, which shows that LMPS has a fast response time, and is suitable for small load applications because of its high sensitivity at low load. The LMPS has a fast response time and is suitable for small signal detection because of its high sensitivity at low load. (Figure 5c) After testing the basic performance of the LMPS, we further conducted a cyclic compression test to determine its durability and stability. We used 35 kPa periodic to load/unload 4000 cycles rapidly, and intercepted 500~550s and 3500~3550s segments, which showed that the LMPS has good stability and the ability to work for a long time. (Figure 5d) In order to understand limitation of the environment in which the sensor is used, we studied the change in capacitance of the sensor at different temperatures and under different loads. As can be seen from the Figure 5e, the sensor is insensitive to changes in temperature under different loads, which is due to the air between the electrodes and the small change in the dielectric constant of the TPU when the temperature changes. Also in order to understand the performance of the sensor, a hysteresis study was conducted as shown in the Figure 5f. The hysteresis response of the sensor is relatively obvious at low loads because the TPU is stiffer leading to its weak resilience performance. The above results illustrate the effectiveness of using laser irradiation to fabricate microstructure on natural wood and wide prospects for LMPS.

3.5. Potential Applications for Human Motion Detection

The potential of the LMPS for human motion detection is demonstrated. As shown in Figure 6a-f, the LMPS is fixed at earwash ball blowing, the face, the joint of a forefinger and the elbow. It can be seen that with airflow, finger flexion, arm bending, knee bending and facial expression of cheek-bulging, the capacitance of the LMPS changes fast and maintains. When the motion stops and returns to the original position, the LMPS removes the compression and the capacitance quickly returns to the initial value. The above experiments show that the LMPS exhibits excellent performance in pressure sensing and motion detection, further demonstrating the great potential of fabrication of LMPS from natural wood in the fields of artificial skin, robotics and flexible sensing.

Preprints (www.preprints.org) | NOT PEER-REVIEWED | Posted: 18 May 2023 doi:10.20944/preprints202305.1313.v1

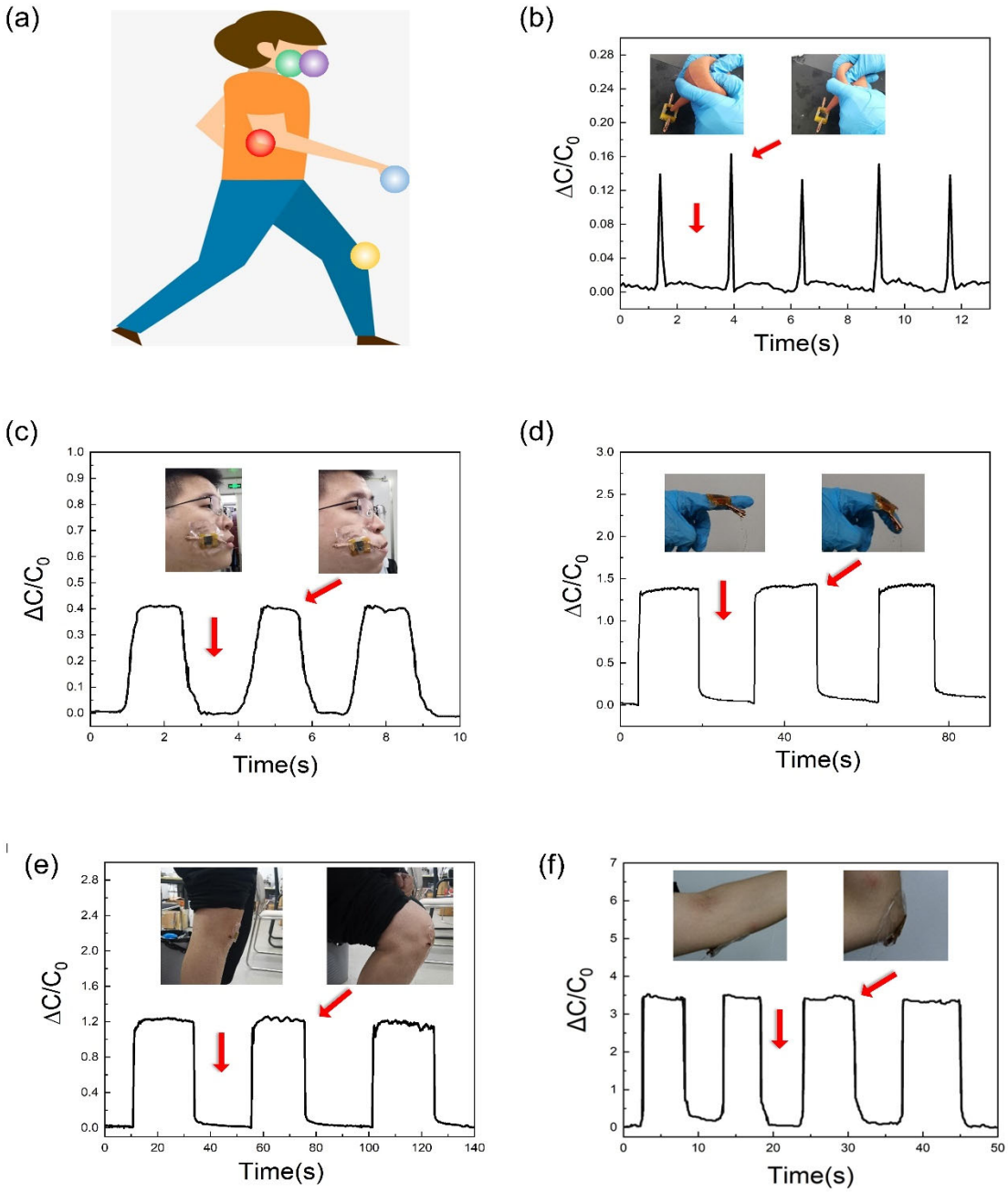

Figure 6. (a) Monitoring human motion with the LMPS at different sites (b) earwash ball blowing, (c) facial expression of cheek-bulging, (d) finger movement, (e) knee bending (f) arm bending.

4. Conclusions

In this paper, we reported a simple, efficient, and fast method to deal with the overall flexibility limitation of the sensor caused by metal electrodes and adhesives by transferring LIG from natural wood as well as microstructures with high sensitivity. In addition, the effects of different processing parameters, such as laser power, scan speed, defocus distance, and flame retardant treatment, on the sheet resistance of the LTE were explored. The LIG generated by optimizing the laser parameters (50% laser power,48mm s^{-1} scan speed and 0.5mm defocus distance) yielded a sheet resistance as low as 14.7 Ω/□. On the basis of this electrode, microstructures were formed on the electrode surface, which further improved the sensitivity of the sensor. The LMPS provides high sensitivity (0.11 kPa^{-1}), ultra-wide pressure detection range (100Pa to 1.4MPa), fast response (~300ms) and good stability (>4000 cycles, at 0-35kPa). This method allows the flexibility of the sensor to be improved and

promotes further development of flexible electronic devices with LIG from laser for more potential applications.

Author Contributions: Conceptualization, C.Q. and B.S.; methodology, C.Q.; software, C.Q. and M.L.; validation, C.Q. and B.S.; formal analysis, Z.Z. and C.Q.; investigation, C.Q., D.Z. and J.W.; resources, B.S.; data curation, C.Q.; writing—original draft preparation, C.Q. and B.S.; writing—review and editing, C.Q. and B.S.; visualization, S.C. and D.L.; supervision, B.S.; project administration, B.S.; funding acquisition, B.S. All authors have read and agreed to the published version of the manuscript.

Funding: This research was funded by the Natural Science Foundation of Shanghai (19ZR1436100) and the National Natural Science Foundation of China (11105149).

Acknowledgments: The authors express gratitude to the editors and the reviewers for their constructive and helpful review comments.

Conflicts of Interest: The authors declare no conflict of interest.

References

1. Khan, H.; Razmjou, A.; Warkiani, M.-E.; Kottapalli, A.; Asadnia, M. Sensitive and Flexible Polymeric Strain Sensor for Accurate Human Motion Monitoring. *Sensors* **2018**, *18*, 418.
2. Wang, Y.; Wang, L.; Yang, T.; Li, X; Zang, X.; Zhu, M.; Wang, K.; Wu, D.; Zhu, K. Wearable and Highly Sensitive Graphene Strain Sensors for Human Motion Monitoring. *Adv. Funct. Mater.* **2014**, *24*, 4666-4670.
3. Yang, Y.-C.; Mun, J.; Kwon, S.-Y.; Park, S.; Bao, Z.; Park, S. Electronic Skin: Recent Progress and Future Prospects for Skin-attachable Devices for Health Monitoring, Robotics, and Prosthetics. *Adv. Mater.* **2019,** *31*, 1904765.
4. Billard, A.; Kragic, D. Trends and Challenges in Robot Manipulation. *Science* **2019,** *364*, 1149.
5. Wang, J.; Wang, N.; Xu, D.; Tang, L.; Sheng, B. Flexible Humidity Sensors Composed with Electrodes of Laser Induced Graphene and Sputtered Sensitive Films Derived from Poly(ether-ether-ketone). *Sensors and Actuators: B. Chemical* **2023**, *375*,132846.
6. Xu, D.; Liu, B.; Wang, N.; Zhou, J.; Tang, L.; Zhang, D.; Sheng, B. Ultrasensitive and flexible humidity sensors fabricated by ion beam sputtering and deposition from polydimethylsiloxane. *Vacuum* **2023**, 213, 112125.
7. Shi, S.; Liang, J.; Qu, C.; Chen, S.; Sheng, B. Ramie Fabric Treated with Carboxymethylcellulose and Laser Engraved for Strain and Humidity Sensing. *Micromachines* **2022**, *13*,1309.
8. Wang, N.; Tong, J.; Wang, J.; Wang, Q.; Chen, S.; Sheng, B. Polyimide-Sputtered and Polymerized Films with Ultrahigh Moisture Sensitivity for Respiratory Monitoring and Contactless Sensing.*ACS Applied Materials & Interfaces* **2022**, *14*, 11842-11853.
9. Wang, D.; Sheng, B.; Peng, L.; Huang, Y.; Ni, Z. Flexible and Optical Fiber Sensors Composited by Graphene and PDMS for Motion Detection. *Polymers* **2019**, *11*, 1433.
10. Tong, J.; Wang, N.; Wang, Q.; Chen, S.; Sheng, B. Improved Sensitive Conductive Sponge Sensors with Tunnel-crack Broadening for Pressure, Humidity and Temperature Sensing Applications. *Sens. Actuators B Chem.* **2022,** *358*, 131497.
11. Horev, Y.-D.; Maity, A.; Zheng, Y.; Milyutin, Y.; Khatib, M.; Yuan, M.; Suckeveriene, R.-Y.; Tang, N.; Wu, W.; Haick, H. Stretchable and Highly Permeable Nanofibrous Sensors for Detecting Complex Human Body Motion. *Adv. Mater.* **2021**, *33*, 2102488.
12. Xiao, J.; Xiong, Y.; Chen, J.; Zhao, S.; Chen, S.; Xu, B.; Sheng, B. Ultrasensitive and Highly Stretchable Fibers with Dual Conductive Microstructural Sheaths for Human Motion and Micro Vibration Sensing. *Nanoscale* **2022** ,*14*, 1962-1970.
13. Xiong, Y.; Xiao, J.; Chen, J.; Xu, D.; Zhao, S.; Chen S.; Sheng, B. Multifunctional Hollow TPU Fiber Filled with Liquid Metal Exhibiting Fast Electrothermal Deformation and Recovery. *Soft Matter* **2021**, *17*, 10016-10024.
14. Wang, Q.; Tong, J.; Wang, N.; Chen, S.; Sheng, B. Humidity Sensor of Tunnel-Cracked Nickel@polyurethane Sponge for Respiratory and Perspiration Sensing. *Sensors and Actuators: B. Chemical* **2021**, *330*, 129322.
15. Jayathilaka, W.; Qi, K.; Qin, Y.; Chinnappan, A.; Serrano-Garcia, W.; Baskar, C.; Wang, H.; He, J.; Cui, S.; Thomas, S.-W.; Ramakrishna, S. Significance of Nanomaterials in Wearables: A Review on Wearable Actuators and Sensors. *Adv. Mater.* **2019,** *31*, 1805921.

16. Liu, Q.; Zhao, S.; Hu, T.; Jiang, C.; Sheng, B. Superstretchable and Linear-Response Strain Sensors With Carbon Nanotubes Ultrasonically Assembled on Silicone Rubber Film. *IEEE Sensors Journal*, Doi:10.1109/JSEN.2023.3254139.
17. Zhao, S.; Chen, J.; Zhou, J.; Shi, S.; Hou, M.; Sheng, B. Superelastic Conductive Fibers with Fractal Helices for Flexible Electronic Applications. *Advanced Materials Technologies*, Doi:10.1002/admt.202201951.
18. Carvalho, A.-F.; Fernandes, A.J.-S.; Martins, R.; Fortunato, E.; Costa, F.-M. Laser-Induced Graphene Piezoresistive Sensors Synthesized Directly on Cork Insoles for Gait Analysis. *Adv. Mater. Technol.* **2020**, 2000630.
19. Lü, X.; Yu, T.; Meng, F.; Bao, W. Wide-Range and High-Stability Flexible Conductive Graphene/Thermoplastic Polyurethane Foam for Piezoresistive Sensor Applications. *Adv. Mater. Technol.* **2021,** *6*, 2100248.
20. Xu, D.; Duan, L.; Yan, S.; Wang, Y.; Cao, K.; Wang, W.; Xu, H.; Wang, Y.; Hu, L.; Gao, L. Monolayer MoS_2-Based Flexible and Highly Sensitive Pressure Sensor with Wide Sensing Range. *Micromachines* **2022**, *13*, 660.
21. Ha, K.; Huh, H.; Li, Z.; Lu, N. Soft Capacitive Pressure Sensors: Trends, Challenges, and Perspectives. *ACS Nano* **2022**, *16*, 3442−3448.
22. Yu, Q.; Zhang, J. Flexible Capacitive Pressure Sensor Based on a Double-Sided Microstructure Porous Dielectric Layer. *Micromachines* **2023**, *14*, 111.
23. Fan, F.-R.; Lin, L.; Zhu, G.; Wu, W.; Zhang, R.; Wang, Z.-L. Transparent Triboelectric Nanogenerators and Self-Powered Pressure Sensors Based on Micropatterned Plastic Films. *Nano Lett.* **2012**, *12*, 3109.
24. Chen, Z.; Wang, Z.; Li, X.; Lin, Y.; Luo, N.; Long, M.; Zhao, N.; Xu, J.-B. Flexible Piezoelectric-Induced Pressure Sensors for Static Measurements Based on Nanowires/Graphene Heterostructures. *ACS Nano* **2017**, *11*, 4507.
25. Wu, W.; Wen, X.; Wang, Z.-L. Taxel-Addressable Matrix of Vertical-Nanowire Piezotronic Transistors for Active and Adaptive Tactile Imaging. *Science* **2013**, *340*, 952.
26. Ji, B.; Zhou, Q.; Chen, G.; Dai, Z.; Li, S.; Xu, Y.; Gao, Y.; Wen, W.; Zhou, B. In Situ Assembly of A Wearable Capacitive Sensor with A Spine-Shaped Dielectric for Shear-Pressure Monitoring. *J. Mater. Chem. C* **2020**, *8*, 15634-15645.
27. Chen, Z.; Zhang, Y.; Zhu, B.; Wu, Y.; Du, X.; Lin, L.; Wu, D. Laser-Sculptured Hierarchical Spinous Structures for Ultra-High Sensitivity Iontronic Sensors with A Broad Operation Range. *ACS Appl. Mater. Interfaces* **2022**, *14*, 19672−19682.
28. Yang, J.; Luo, S.; Zhou, X.; Li, J.; Fu, J.; Yang, W.; Wei, D. Flexible, Tunable, and Ultrasensitive Capacitive Pressure Sensor with Microconformal Graphene Electrodes. *ACS Appl. Mater. Interfaces* **2019**, *11*, 14997−15006.
29. Qin, J.; Yin, L.; Hao, Y.; Zhong, S.; Zhang, D.; Bi, K.; Zhang, Y.; Zhao, Y.; Dang, Z. Flexible and Stretchable Capacitive Sensors with Different Microstructures. *Adv. Mater.* **2021**, *33*, 2008267.
30. Luo, Y.; Shao, J.; Chen, S.; Chen, X.; Tian, H.; Li, X.; Wang, L.; Wang, D.; Lu, B. Flexible Capacitive Pressure Sensor Enhanced by Tilted Micropillar Arrays. *ACS Appl. Mater. Interfaces* **2019**, *11*, 17796−17803.
31. Ji, B.; Zhou, Q.; Lei, M.; Ding, S.; Song, Q.; Gao, Y.; Li, S.; Xu, Y.; Zhou, Y.; Zhou, B. Gradient Architecture-Enabled Capacitive Tactile Sensor with High Sensitivity and Ultrabroad Linearity Range. *Small* **2021**, 17, 2103312.
32. Ruth, S.R.-A.; Beker, L.; Tran, H.; Feig, V.-R.; Matsuhisa, N.; Bao, Z. Rational Design of Capacitive Pressure Sensors Based on Pyramidal Microstructures for Specialized Monitoring of Biosignals. *Adv. Funct. Mater.* **2019**, *30*, 1903100.
33. Le, T.-D.; Phan, H.; Kwon, S.; Park, S.; Jung, Y.; Min, J.; Chun, B.-J.; Yoon, H.; Ko, S.-H.; Kim, S.; Kim, Y. Recent Advances in Laser-Induced Graphene: Mechanism, Fabrication, Properties, and Applications in Flexible Electronics. *Adv. Funct. Mater.* **2022**, *32*, 2205158.
34. Lin, J.; Peng, Z.; Liu, Y.; Ruiz-Zepeda, F.; Ye, R.; Samuel, E.L.-G.; Yacaman, M.-J.; Yakobson, B.-I.; Tour, J.-M. Laser-Induced Porous Graphene Films from Commercial Polymers. *Nat. Commun.* **2014**, *5*, 5714.
35. Kulyk, B.; Silva, B.F.-R.; Carvalho, A.-F.; Silvestre, S.; Fernandes, A.J.-S.; Martins, R.; Fortunato, E.; Costa, F.-M. Laser-Induced Graphene from Paper for Mechanical Sensing. *ACS Appl. Mater. Interfaces* **2021**, *13*, 10210−10221.
36. You, R.; Liu, Y.; Hao, Y.; Han, D.; Zhang, Y.; You, Z. Laser Fabrication of Graphene-Based Flexible Electronics. *Adv. Mater.* **2020**, *32*, 1901981.
37. Ye, R.; Chyan, Y.; Zhang, J.; Li, Y.; Han, X.; Kittrell, C.; Tour, J.-M. Laser-Induced Graphene Formation on Wood. *Adv. Mater.* **2017**, *29*, 1702211.
38. Le, T.-D.; Park, S.; An, J.; Lee, P.-S.; Kim, Y. Ultrafast Laser Pulses Enable One-Step Graphene Patterning on Woods and Leaves for Green Electronics. *Adv. Funct. Mater.* **2019**, *29*, 1902771.
39. Chyan, Y.; Ye, R.; Li, Y.; Singh, S.-P.; Arnusch, C.-J.; Tour, J.-M. Laser-Induced Graphene by Multiple Lasing: Toward Electronics on Cloth, Paper, and Food. *ACS Nano* **2018**, *12*, 2176−2183.
40. Guo, H.; Yan, J.; Jiang, L.; Qu, L.; Yin, J.; Lu, J. Conductive Writing with High Precision by Laser-Induced Point-to-Line Carbonization Strategy for Flexible Supercapacitors. *Adv. Optical Mater.* **2021**, *9*, 2100793.

41. Shintake, J.; Piskarev, Y.; Jeong, S.-H.; Floreano, D. Ultrastretchable Strain Sensors Using Carbon Black-Filled Elastomer Composites and Comparison of Capacitive Versus Resistive Sensors. *Adv. Mater. Technol.* **2018**, *3*, 1700284.
42. Zhu, J.; Huang, X.; Song, W. Physical and Chemical Sensors on the Basis of Laser-Induced Graphene: Mechanisms, Applications, and Perspectives. *ACS Nano* **2021**, *15*, 18708−18741.
43. Xu, Y.; Fei, Q.; Page, M.; Zhao, G.; Ling, Y.; Chen, D.; Yan, Z. Laser-Induced Graphene for Bioelectronics and Soft Actuators. *Nano Res.* **2021**, *14*, 3033–3050.
44. Kulyk, B.; Silva, B.F.-R.; Carvalho, A.-F.; Barbosa, P.; Girão, A.-V.; Deuermeier, J.; Fernandes, A.J.-S.; Figueiredo, F.M.-L.; Fortunato, E.; Costa, F.-M. Laser-Induced Graphene from Paper by Ultraviolet Irradiation: Humidity and Temperature Sensors. *Adv. Mater. Technol.* **2022**, 7, 2101311.
45. Hong, J.; Wu, J.; Mao, Y.; Shi, Q.; Xia, J.; Lei, W. Transferred Laser-Scribed Graphene-Based Durable and Permeable Strain Sensor. *Adv. Mater. Interfaces* **2021**, *8*, 2100625.
46. Du, Q.; Liu, L.; Tang, R.; Ai, J.; Wang, Z.; Fu, Q.; Li, C.; Chen, Y.; Feng, X. High-Performance Flexible Pressure Sensor Based on Controllable Hierarchical Microstructures by Laser Scribing for Wearable Electronics. *Adv. Mater. Technol.* **2021**, *6*, 2100122.
47. Lamberti, A.; Clerici, F.; Fontana, M.; Scaltrito, L. A Highly Stretchable Supercapacitor Using Laser-Induced Graphene Electrodes onto Elastomeric Substrate. *Adv. Energy Mater.* **2016**, *6*, 1600050.
48. Gao, Y.; Lu, C.; Guohui, Y.; Sha, J.; Tan, J.; Xuan, F. Laser Micro-Structured Pressure Sensor with Modulated Sensitivity for Electronic Skins. *Nanotechnology* **2019**, *30*, 325502.
49. Madyaratri, E.-W.; Ridho, M.-R.; Aristri, M.-A.; Lubis, M.A.-R.; Iswanto, A.-H.; Nawawi, D.-S.; Antov, P.; Kristak, L.; Majlingová, A.; Fatriasari, W. Recent Advances in the Development of Fire-Resistant Biocomposites—A Review. *Polymers* **2022**, *14*, 362.
50. Chen, C.; Hu, L. Nanoscale Ion Regulation in Wood-Based Structures and Their Device Applications. *Adv. Mater.* **2021**, *33*, 2002890.
51. Mannion, P.-T.; Magee, J.; Coyne, E.; O'Connor, G.-M.; Glynn, T.-J. The Effect of Damage Accumulation Behaviour on Ablation Thresholds and Damage Morphology in Ultrafast Laser Micro-Machining of Common Metals in Air. *Appl. Surf. Sci.* **2004**, *233*, 275-287.
52. Ma, C.; Li, G.; Qin, L.; Huang, W.; Zhang, H.; Liu, W.; Dong, T.; Li, S. Analytical Model of Micropyramidal Capacitive Pressure Sensors and Machine-Learning-Assisted Design. *Adv. Mater. Technol.* **2021**, 6, 2100634.